DNA Polymerase Photoprobe 2-[(4-Azidophenacyl)thio]-2′-deoxyadenosine 5′-Triphosphate Labels an *Escherichia coli* DNA Polymerase I Klenow Fragment Substrate Binding Site[†,‡]

Bob M. Moore, II,[§] Ravi K. Jalluri, and Michael B. Doughty*

Department of Medicinal Chemistry, The University of Kansas, Lawrence, Kansas 66045

Received October 20, 1995; Revised Manuscript Received May 7, 1996[⊗]

ABSTRACT: The nucleotide photoprobe 2-[(4-azidophenacyl)thio]-2′-deoxyadenosine 5′-triphosphate (**1**) was evaluated as a photoaffinity label of the DNA polymerase I Klenow fragment. Photolabel [^{3}H]-**1** covalently labeled the Klenow fragment with photolysis at 300 nm, reaching saturation at an approximate 1:1 mole ratio at 5.7 μM and with an EC_{50} (the effective concentration at 50% maximum photoincorporation) of about 0.74 μM. Saturating concentrations of poly(dA)·$(T)_{10}$ protect the Klenow fragment from [^{3}H]-**1** photoincorporation, and TTP at a concentration approximately equal to its K_D for the free enzyme form shifts the dose−response curve for photoincorporation of [^{3}H]-**1** into the Klenow fragment by a factor of 2, indicating a competitive relationship between TTP and **1**. Additionally, the photoincorporation of [^{3}H]-**1** into the Klenow fragment has an absolute requirement for magnesium, with no significant photoincorporation observed at concentrations of **1** up to 10 μM in the absence of magnesium. These results demonstrate that, as designed, photoprobe **1** binds to both the dNTP and a portion of the template-primer binding sites on the Klenow fragment. Photoaffinity labeling of the Klenow fragment by **1** yielded a single radiolabeled tryptic fragment which was isolated by HPLC; sequence analysis identified Asp^{732} in the peptide fragment Asp^{732}-Ile^{733}-His^{734}-Arg^{735} as the site of covalent modification. Molecular modeling and complementary NMR analysis of the conformation of **1** indicated preferred C_3′-exo and C_2′-exo-C_3′-endo symmetrical twist furanose ring puckers, with a high antibase conformation and a +sc C-5 torsional angle. Docking studies using Asp^{732} as an anchor point for the azide α-nitrogen on the photolabel indicate that the dNTP binding site is at the edge of the DNA binding cleft opposite the exonuclease site and that the template binding site includes helix O in the finger motif of the Klenow fragment.

DNA polymerase I (Pol I)[1] from *Escherichia coli* was discovered by Kornberg and colleagues in 1956 and was shown to be required *in vivo* for template-driven DNA replication and repair (Kornberg et al., 1956). The isolation and sequencing of the pol I gene (*polA*) led to identification of the complete amino acid sequence (Brown et al., 1982; Joyce et al., 1982). The enzyme consists of a single polypeptide chain having 928 amino acid residues with a molecular mass of 103 kDa, and the enzyme is active as the monomer. Limited subtilisin cleavage of Pol I yields a small 35 kDa fragment with 5′−3′ exonuclease activity and a large 68 kDa fragment referred to as the Klenow fragment with 3′−5′ exonuclease and polymerase activities (Klenow et al., 1971). The Klenow fragment has been the object of extensive kinetic (Bryant et al., 1983; Carroll & Benkovic, 1990; Mizrahi et al., 1985), X-ray crystallographic (Beese et al., 1993a,b; Ollis et al., 1985), affinity labeling (Pandey et al., 1987, 1994a; Pandey & Modak, 1988; Rush & Konigsberg, 1990), and mutagenesis (Astatke et al., 1995; Desai et al., 1994; Pandey et al., 1994b; Polesky et al., 1990, 1992) studies.

The Klenow fragment catalyzes a sequential-ordered reaction where template-primer binds to form a binary complex followed by binding of a complementary 2′-deoxynucleoside 5′-triphosphate (dNTP) (Bryant et al., 1983; Carroll & Benkovic, 1990; Mizrahi et al., 1985). A rate-limiting conformational change occurs in the ternary complex, followed by nucleophilic attack by the 3′-hydroxy primer terminus on the α-phosphate of the dNTP, forming a diester bond and a one-base-extended primer and pyrophosphate. In the second rate-limiting step, the enzyme reverts to its original conformation followed by product release. The Klenow fragment can add deoxynucleotides to a 3′-primer end in a processive manner, although the degree of processivity is dependent on the nature of the template and primer (Bambara et al., 1976, 1978).

X-ray crystal structures of the Klenow fragment indicate at least two different conformational states, a "relaxed" state obtained from high salt in the absence of template-primer or dNTP substrates (Ollis et al., 1985) and a "tight" state (Figure 1) observed in the presence of either of these substrates under conditions of lower salt (Beese et al., 1993a,b). Both forms of the Klenow fragment contain several domains, including the α/β structure of the exonuclease site (β-strands 1−4 and helices A−G) and the deep cleft containing the finger (α-helices L−P), palm (β-sheet

[†] This work was supported by grants from the U.S. Public Health Service (GM38722 and GM07775).

[‡] Taken in part from the Ph.D. dissertation of Bob M. Moore, II, The University of Kansas, Lawrence, KS 66045, 1995.

* Address correspondence to Michael B. Doughty, Department of Medicinal Chemistry, The University of Kansas, Lawrence, KS 66045. Fax: 913-864-5326. Phone: 913-864-4561. E-mail: doughty@kuhub.cc.ukans.edu.

[§] Present address: Drug Design Institute, College of Pharmacy, The University of Texas, Austin, Texas 78713.

[⊗] Abstract published in *Advance ACS Abstracts,* July 1, 1996.

[1] Abbreviations: Pol I, DNA polymerase I; dNTP, 2′-deoxynucleotide 5′-triphosphate; NOE, nuclear Overhauser enhancement; ROESY, rotating frame Overhauser enhancement spectroscopy.

S0006-2960(95)02515-3 CCC: $12.00

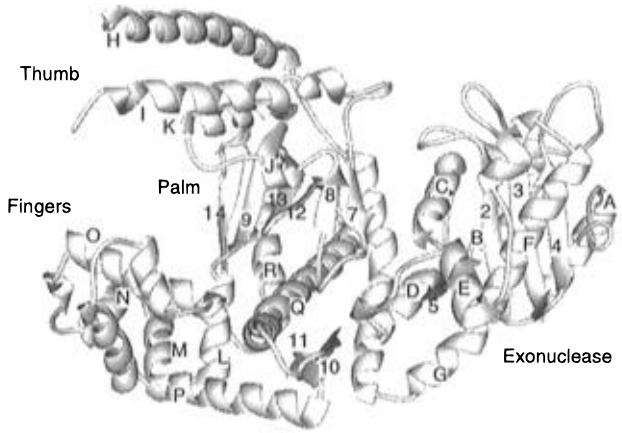

FIGURE 1: Ribbon and cylinder representation of the crystal structure of the *E. coli* DNA polymerase I Klenow fragment (Beese et al., 1993b). The spiral ribbons represent α-helices, the ribbon arrows represent β-strands, and the thin tubes represent turns, loops, and random structures.

strands 7−9 and 12−14), and thumb (α-helices H−K) motifs of the proposed polymerase domain. The Klenow structure also contains three carboxylates—Asp^{705}, Asp^{882}, and Glu^{883}—located in the base of the palm region on β-strands 9, 12, and 13 that are highly conserved across DNA polymerases (Delarue et al., 1990) and that are required for polymerase activity (Beese et al., 1993a; Polesky et al., 1992). However, in a cocrystal structure with the Klenow fragment, double-stranded DNA binds in the exonuclease site, such that this enzyme structure can be considered an editing complex (Beese et al., 1993a). Thus, the orientation of template-primer in the polymerase site is still unknown, and this subject has been the object of extensive debate (Pelletier, 1994; Steitz et al., 1994). Similarly, although a cocrystal structure of the Klenow fragment with dCTP in the absence of template-primer has been determined, the dCTP interaction with helix O places the triphosphate a considerable distance from the carboxylate triad required for catalysis, so the relevance of this orientation to the catalytic mechanism and to the structure of the ternary complex of the Klenow fragment was questioned (Beese et al., 1993b).

Joyce and Steitz (1994) defined several of the difficult problems encountered in defining the dNTP binding site in DNA polymerase I. Although dNTPs bind to the free enzyme form, this binary complex is inhibitory and not catalytic, and because the dNTP binding site in the ternary complex is defined by interactions with the template as well as with the enzyme, the dNTP binding in the absence of template-primer may be sloppy. Thus, although the crystal structure (Beese et al., 1993b), NMR studies (Mullen et al., 1990), and a nucleotide photolabeling study (Rush & Konigsberg, 1990) defined interactions of the dNTP base with residues at the C-terminal end of helix O, these may be important interactions only in the absence of template-primer. The thermodynamic model of substrate interactions in the Klenow fragment (Yadav et al., 1992a) suggest similar problems since the dNTP binding interactions are dominated by the triphosphate and base-pairing interactions, and the remaining interactions may not be sufficient to hold the dNTP in its catalytic position in the binary enzyme−dNTP complex. Similar difficulties arise in site-directed mutagenesis studies where changes in template-primer binding may also have dramatic effects on dNTP binding.

In the previous paper, we outlined an alternative approach for investigating the substrate binding sites in DNA polymerases (Moore et al., 1996). We designed nucleotide photoprobes that tethered aryl azides into the corresponding template binding domain, thus attempting to photolabel amino acid residues in the template binding site complementary to the dNTP binding site. In this series of photoprobes, the tether length is apparently critical to Klenow fragment inhibitory activity, with 2-[(4-azidophenacyl)thio]-2′-deoxyadenosine 5′-triphosphate (**1**), which has a three-atom tether, being the best irreversible photoprobe, with an IC_{50} of about 2 μM for photoinactivation of about 92% of the Klenow fragment polymerase activity. We now report

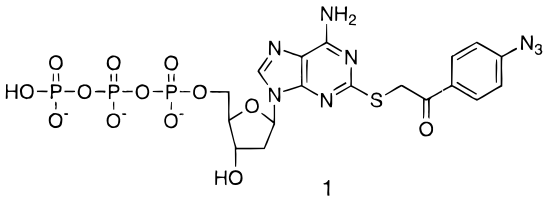

1

that nucleotide **1** photolabels a unique fragment in a proposed template binding domain of the Klenow fragment.

EXPERIMENTAL PROCEDURES

The Klenow fragment was purchased from Worthington Biochemical (Freehold, NJ); trypsin (type XIII, TPCK-treated) was purchased from Sigma (St. Louis, MO), and thymidine triphosphate and poly(dA)·$(T)_{10}$ were purchased from Pharmacia (Piscataway, NJ). Amplify and Hyperfilm-MP were obtained from Amersham (Arlington Heights, IL), and all other reagents were analytical or molecular biology grade. Whatman DE81 [(diethylamino)ethyl]cellulose sheets and Scintiverse II were purchased from Fisher Scientific (Pittsburgh, PA). Spectra/Por dialysis tubing (sulfide and heavy metal free) was purchased from Sigma. The nucleotide photoprobes 2-[(4-azidophenacyl)thio]-2′-deoxyadenosine 5′-tri- (**1**) and monophosphate (**1m**) were synthesized as described (Moore et al., 1996).

Liquid scintillation counting was performed in a Packard 1900 TR Liquid Scintillation Counter (Meridian, CT). Photolysis was conducted in a Rayonet Photochemical Mini-Reactor chamber Model RMR-600 purchased from the Southern New England Ultraviolet Co. (Branford, CT). Photolysis was conducted in 700 μL or 15 mL siliconized, quartz, water-jacketed cells prepared in this lab from Vycor tubing. Gel electrophoresis was performed on a Protean II unit, and gels were dried on a Model 543 gel drier from Bio-Rad (Richmond, CA). Reverse phase high-performance liquid chromatography was conducted on a Beckman gradient mixing system equipped with System Gold software (Fullerton, CA). Amino acid sequence analysis was contracted to the Kansas State University Biotech Core Facility.

*Synthesis of [8-^{3}H]-2-[(4-Azidophenacyl)thio]-2′-deoxyadenosine 5′-Triphosphate ([^{3}H]-**1**).* Nucleotide **1** (3.1 mg, 4.39 μmol) was dissolved in 220 μL of 200 mM AMPSO buffer (pH 9.4), and the solution was lyophilized to dryness. The mixture was treated with 200 μL of ^3H_2O (1 Ci, stock 5 Ci/mL) according to the general procedure of Shelton and Clark (1967). The solution was placed in a heating block equilibrated at 70 °C, and after 24 h, the ^3H_2O was removed *in vacuo* into a sealed trap cooled with liquid nitrogen.

Residual tritium was removed by washing with 3 volumes of water. The dry residue was then dissolved in 200 μL of H_2O and purified by reverse phase HPLC using a Vydac C_{18} semipreparative column, eluting with 20 mM triethylammonium bicarbonate buffer (pH 7.3) in 19% acetonitrile at a flow rate of 2.3 mL/min; effluent was monitored at 275 nm. All three peaks corresponding to the mono-, di-, and triphosphates were collected and lyophilized, yielding 1.45 μmol (33%) of fractions as follows: 413 μg (14%) of triphosphate with a specific activity of 42.7 cpm/pmol, 462 μg (15%) of diphosphate with a specific activity of 51.5 cpm/pmol, and 38 μg (17%) of monophosphate with a specific activity of 55.5 cpm/pmol.

*Photoincorporation of [^{3}H]-**1** into the Klenow Fragment.* DTT was removed from the stock enzyme to prevent aryl azide reduction by dialysis against 50 mM potassium phosphate buffer (pH 7.0) containing 2 mM β-mercaptoethanol and 50% glycerol using Spectra/Por dialysis tubing (molecular weight cutoff of 10 000) at 10 °C over 24 h. Photolysis mixtures contained 0.1 μM Klenow fragment in Tris-HCl buffer (pH 7.5) containing 2.5 mM $MgCl_2$ and 2 mM β-mercaptoethanol in the presence of 0.95, 1.82, 2.61, 5.83, and 9.52 μM [^{3}H]-**1**. Aliquots of each sample were stored on ice as a control, and the remaining were preequilibrated at 37 °C and then photolyzed at 300 nm for 5 min at 37 °C. Samples from photolysis mixtures and control solutions were made basic by the addition of concentrated ammonium hydroxide and spotted in duplicate on 2 × 2 cm^2 swatches of DEAE ion exchange paper. The papers were washed three times with 250 mL of 150 mM ammonium formate (pH 8.0) for 30 min each wash, dehydrated with 95% ethanol, and washed with ether. The squares were air-dried and then counted in Scintiverse II (5 mL) for 5 min. For protection studies, the above experiments were repeated in the presence of 30 μM TTP or 200 nM poly(dA)·$(T)_{10}$. The fraction of [^{3}H]-**1** incorporated into the Klenow fragment was calculated from specific incorporation ($cpm_{photolyzed} - cpm_{unphotolyzed}$) times the specific activity of [^{3}H]-**1** in counts per minute per picomole divided by the picomoles of Klenow fragment. This incorporation data was analyzed as EC_{50}, i.e., the effective concentration of label yielding 50% of maximum photoincorporation, and fit to eq 1,

$$\frac{[E_I]}{[E_T]} = \frac{f[I]}{[I] + K_{D,app}} \quad (1)$$

where $[E_I]/[E_T]$ is the mole fraction of [^{3}H]-**1**−Klenow fragment covalent adduct, f is the maximum fraction of enzyme labeled, [I] is the concentration of [^{3}H]-**1**, and $K_{D,app}$ is the apparent dissociation constant for the E−I complex. The dissociation constant $K_{D,app}$ was estimated by fitting the data to eq 1 by nonlinear regression analysis using the program MINSQ (MicroMath, Salt Lake City, UT).

*Photoaffinity Labeling of the Klenow Fragment by [^{3}H]-**1**.* A mixture containing 63 mM Tris-HCl buffer (pH 7.5) containing 2.5 mM $MgCl_2$, 2 mM β-mercaptoethanol, 6 μM [^{3}H]-**1**, and 0.1 μM Klenow fragment was equilibrated at 37 °C for 15 min in a 15 mL quartz photolysis cell. The mixture was then photolyzed for 15 min at 300 nm, and the solution was lyophilized to dryness. The resulting pellet was dissolved in water (100 μL) and the solution transferred to dialysis tubing (Spectra/Por, molecular weight cutoff of 10 000) and dialyzed against three 300 mL changes of 150 mM ammonium bicarbonate (pH 7.0) containing 2 mM β-mercaptoethanol at 10 °C over 27 h. The solution was then lyophilized in a siliconized polyethylene tube.

The resulting pellet was dissolved in a solution of 50 mM ammonium bicarbonate containing 680 ng of trypsin (a 1:50 trypsin to Klenow fragment ratio), and the solution was incubated for 2 h at 37 °C. An additional 680 ng of trypsin was added after 2 h, and the incubation was continued for 18 h. The trypsin digest was centrifuged and then separated by reverse phase high-performance liquid chromatography on a Vydac C_{18} analytical reverse phase column using a gradient elution from 0.1% TFA (buffer A) to 0.1% TFA in 50% acetonitrile (buffer B) over 60 min at a flow rate of 0.7 mL/min, and the eluant was monitored at 220 nm. Fractions from 24 to 29 min were collected at 1 min intervals, and aliquots (14%) were counted for radioactivity. Fractions comprising the single peak of radioactivity were pooled, lyophilized in a siliconized polyethylene tube, and subjected to HPLC with a gradient running from 0 to 60% B over 60 min. A single peak containing radioactivity was collected and sequenced using automated Edman degradation chemistry.

*Gel Electrophoresis of [^{3}H]-**1**-Photolabeled Klenow Fragment.* Photolabeling was performed as described in the previous section using 260 pmol of the Klenow fragment. The photolysis mixture was lyophilized to dryness and reconstituted in 20 μL of water. This mixture was divided into two samples (40 and 220 pmol), treated with 2× treatment buffer containing 0.125 M Tris-HCl buffer (pH 6.8) containing 4% SDS, 20% glycerol, 10% β-mercaptoethanol, and bromophenol blue, and boiled for 1 min. The samples were subjected to denaturing gel electrophoresis using the methodology of Laemmli (1958). The small sample was stained for protein with Coomassie blue, and the large sample was treated with Amplify and subjected to fluoroautoradiography for 2.5 months at −78 °C to detect radioactivity.

Computational Methods. Molecular mechanics, semiempirical calculations, and molecular modeling were performed on an IBM RS/6000 Workstation Model 560 running IBM's UNIX variant AIX (version 4.25). The modeling software used was the Sybyl program package (version 6.01) from Tripos Associates, Inc. (St. Louis, MO). A model of the substituted photoprobe base was constructed using bond lengths and bond angles from similar compounds (Lumbroso et al., 1989; Tomer et al., 1988). Charges for the substituted bases were determined by MNDO semiempirical calculations (MOPAC). Minimum energy conformations were determined from grid searches on the tether torsional angles over a 360° cycle at 3° increments. Minimizations at each iteration were performed in the Tripos force field using the Powell optimization procedure.

A model of photoprobe **1** was constructed from the minimized substituted base (minus azide), a staggered triphosphate (Montaudo et al., 1971; Sorriso et al., 1974) adjusted according to crystal structure data for sodium triphosphate (Davies & Corbridge, 1958) and 2′-deoxyadenosine 5′-triphosphate bound to rat β polymerase (Sawaya et al., 1994), and a C_2′-endo or C_3′-endo furanose conformation taken from B-DNA or RNA, respectively. The initial models were minimized using the Kollman force field supplemented by anomeric parameters (Jalluri et al., 1993). Minimum energy furanose conformations were determined

from sequential grid searches from τ_2 to τ_1 (driving τ from −40 to 40° for the C_2'-endo conformer and 40 to −40° for the C_3'-endo conformer) utilizing the modified Kollman force field minimization procedure. Molecules resulting from grid searches were collected in a molecular spreadsheet. The energy was calculated using the Kollman force field, and the pseudorotational phase angle was calculated using eq 2,

$$\tan P = \frac{(\tau_4 + \tau_1 - \tau_3 - \tau_0)}{(3.078\tau_2)} \qquad (2)$$

where P is the pseudorotational angle and $\tau_0-\tau_4$ are the endocyclic torsional angles (Altona & Sundaralingam, 1972; Levitt & Warshel, 1978; Westhof & Sundaralingam, 1980).

The potential energy profiles for χ (the $O_4'-C_1'-N_9-C_4$ torsional angle in purines) and γ (the $O_5'-C_5'-C_4'-C_3'$ torsional angle) were determined by setting γ in the +sc or ap conformations and conducting grid searches about χ from 0° in a clockwise direction. The resulting molecules were collected in a molecular spreadsheet, and the energies were determined as a function of χ at a fixed γ torsional angle. The energy minimum structures of **1** were docked into the crystal structure of the Klenow fragment (Beese et al., 1993b) in Sybyl (Tripos) and in the MidasPlus program package (Ferrin et al., 1988) obtained from the Computer Graphics Laboratory, University of California, San Francisco (supported by NIH Grant RR-01081) on IBM RS/6000 and Silicon Graphics Indigo workstations, respectively, and graphics images were produced from both software packages.

Nuclear Magnetic Resonance Spectroscopy. All NMR experiments were performed on a Bruker AM 500 spectrometer in 99% D_2O at photoprobe concentrations of 2−6 mM. Coupling constants for the furanose ring protons were obtained by sequential decoupling of each proton; data were collected at 288, 298, and 306 K. Phase angles, puckers, and relative conformational populations of the furanose ring were calculated by fitting the coupling data to the generalized Karplus equation modified to account for electronegativity of β substituents using the program PSEUROT (Altona & Sundaralingam, 1972). Our laboratory modified the program to run in a DOS environment and to perform global evaluations on endocyclic ^3J(H,H) sets.

Phase sensitive, time proportional phase incrementation two-dimensional ROESY spectra were obtained at a 500 ms mixing time with 64 scans/block containing four dummy scans for 256 blocks, a 4000 Hz sweep width, and a 2 s relaxation between scans, collecting 2K data points. Data were transferred to a Silicon Graphics Indigo workstation and Fourier transformed using Felix NMR data-processing software (Biosym, San Diego, CA). Data were multiplied by a 90° phase-shifted squared sine bell function in both dimensions.

RESULTS

*Photoincorporation of [^{3}H]-**1** into the Klenow Fragment and Substrate Protection.* The Klenow fragment was photolyzed for 5 min at 300 nm in the presence or absence of 2.5 mM $MgCl_2$; the enzyme was bound to DEAE paper, and covalently attached [^{3}H]-**1** was determined by liquid scintillation counting following extensive washing to remove reversibly bound photoprobe. Figure 2 shows saturable photoincorporation of [^{3}H]-**1** where an approximate 1:1 mole ratio of photoprobe to Klenow fragment is achieved at 5.8 μM [^{3}H]-**1** with an EC_{50} of about 0.75 μM; however, photoincorporation is completely abolished in the absence of $MgCl_2$. A model for the concentration dependence of photoincorporation was derived from the law of mass action assuming that photoincorporation occurs from an enzyme−photoprobe binary complex (eq 1). The model assumes that photoprobe binding is specific and saturable, that photoproducts of aryl azide decomposition do not inhibit photoincorporation, and that photoprobe depletion during photolysis has no significant effect on the reversible steady state enzyme−photoprobe equilibrium. Using these assumptions and on the basis of the mole ratio of irreversibly bound [^{3}H]-**1** to Klenow fragment, the reversible enzyme−photoprobe complex was calculated to have a $K_{D,app}$ of 1.0 μM. It should be noted, however, that the photoproducts may in fact inhibit the photoincorporation, such that this method may underestimate the $K_{D,app}$ since a competitive inhibitor would shift the dose−response curve to higher concentration.

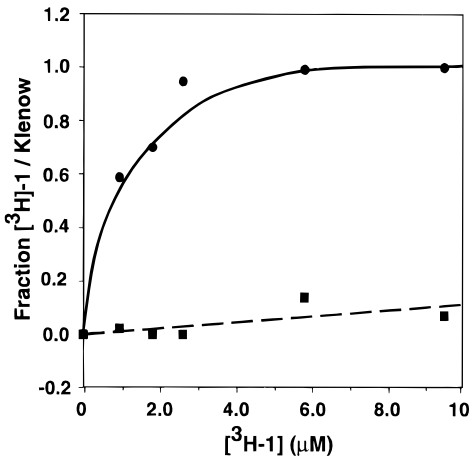

FIGURE 2: Photoincorporation of [^{3}H]-**1** into the Klenow fragment in the presence (circles) and absence (squares) of 2.5 mM $MgCl_2$. Assays were performed in 62.8 mM Tris-HCl buffer (pH 7.5) containing 2 mM β-mercaptoethanol, 10 pmol of the Klenow fragment, and variable concentrations of [^{3}H]-**1** at 37 °C with photolysis at 300 nm for 5 min. Irreversible incorporation was quantified using a DEAE absorption assay as described in Experimental Procedures. The solid line represents the best fit to eq 1 of the data in the presence of magnesium.

Photoincorporation of [^{3}H]-**1** into the Klenow fragment was also examined in the presence of both poly(dA)·$(T)_{10}$ and TTP (Figure 3); in the presence of 200 nM poly(dA)·$(T)_{10}$, i.e., at about 10 times its K_D concentration (Bryant et al., 1983), photoincorporation of [^{3}H]-**1** was completely abolished. Thymidine triphosphate at 30 μM, i.e., at the approximate K_D for dNTP binding to the free enzyme, afforded high protection from photoincorporation at low concentrations of [^{3}H]-**1**, a protection that was reversed at high concentrations of [^{3}H]-**1**.

Photoaffinity labeling of the Klenow fragment by [^{3}H]-**1** was carried out on the basis of the photoincorporation results. Incubation of 1500 pmol of Klenow fragment with 6 μM [^{3}H]-**1** followed by photolysis at 300 nm resulted in 1494 pmol of irreversibly bound radioactivity as determined using the DEAE absorption assay. After dialysis, 90% of the mixture was digested with trypsin and the tryptic fragments were separated by reverse phase HPLC (Figure 4). Radioactivity (536 pmol total or 40% of the initial) was detected as a single peak eluting in fractions from 24 to 29 min.

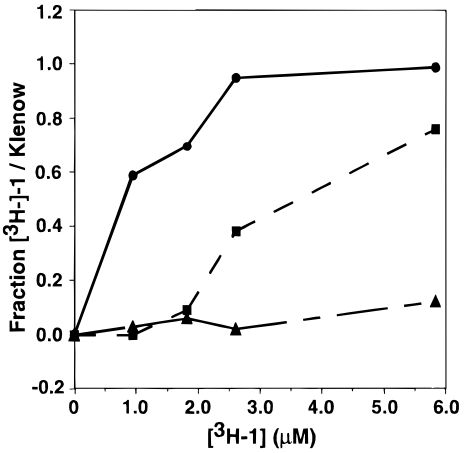

FIGURE 3: Photoincorporation of [^{3}H]-**1** into the Klenow fragment in the absence (circles) and presence of 30 μM TTP (squares) or 200 nM poly(dA)·(T)$_{10}$ (triangles). Assays were performed as described in the legend to Figure 2.

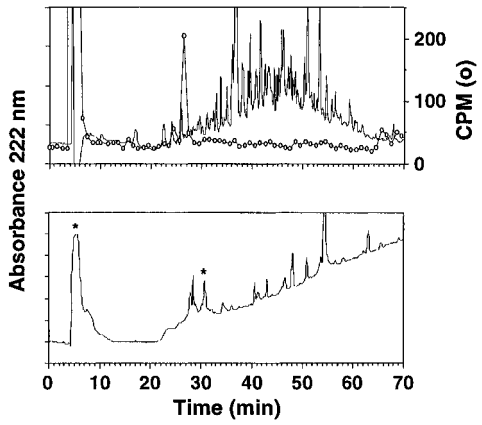

FIGURE 4: (Top) HPLC elution profiles for a tryptic digest of [^{3}H]-**1**-labeled Klenow fragment. The fragments were eluted from a C_{18} analytical reverse phase column with a 0 to 50% acetonitrile gradient in 0.1% TFA over 60 min at 0.7 mL/min. Fractions were collected at 1 min intervals, and a portion was counted for radioactivity (circles). (Bottom) Chromatography of the 24−29 min fraction from the above chromatogram. The fragments were eluted from a C_{18} analytical reverse phase column with a gradient from 0 to 30% acetonitrile in 0.1% TFA for 60 min. Radioactive fractions are marked with an asterisk.

Rechromatography of this pooled fraction resulted in the isolation of a single peak containing 57 pmol of irreversibly bound [^{3}H]-**1** in a peak eluting at 30.5 min (Figure 4); in addition, 110 pmol of radiolabel eluted in the injection volume. Including all of the radioactivity recovered, the isolation yield was 34% as calculated relative to the peak collected in the first HPLC purification. The labeled trypsin fragment was sequenced using Edman degradation chemistry. The amino acid sequence of the tryptic fragment was X-I-H-R (Table 1), where X does not correspond to a natural amino acid. This photolabeled fragment corresponds uniquely to the sequence D^{732}-I^{733}-H^{734}-R^{735} located in helix N of the Klenow fragment, and because the majority of the radioactivity eluted in the first cycle, we conclude that the site of incorporation is Asp^{732}.

Irreversible incorporation of [^{3}H]-**1** into the Klenow fragment was independently verified by denaturing gel electrophoresis. Aliquots of the Klenow fragment photolabeled with [^{3}H]-**1** were subjected to denaturing gel electrophoresis; one sample was stained for protein with Coomassie blue, and a second sample was subjected to fluoroautoradiography. The Coomassie-stained gel contained a single protein band at 68 kDa (R_f = 0.18) that comigrated with a stock Klenow fragment sample. Additionally, a single band containing radioactivity (R_f = 0.18) was detected by fluoroautoradiography. Therefore, the results of gel electrophoresis correlate with the covalent attachment of [^{3}H]-**1** to the Klenow fragment observed in the photoaffinity labeling studies.

Table 1: Sequence Data on the Tryptic Fragment Isolated by Reverse Phase HPLC

sequencing cycle	amino acid observed	predicted sequence	yield[a] (pmol)	radioactivity[b] (cpm)
1	X	D^{732}		305
2	I	I^{733}	26	73
3	H	H^{734}	13	92
4	R	R^{735}	10	85
5	−	−	−	93

[a] Yield of the PTH derivative based on peak area relative to that of a 30 pmol sample. [b] Total radioactivity eluted with the PTH amino acids for each cycle.

*Modeling Studies on the Low-Energy Conformations of Photoprobe **1**.* Molecular mechanics calculations on tether torsional angles in 2-[(4-azidophenacyl)thio]adenine predicted geometries similar to that of α-methylthioacetophenone and acetophenone (Lumbroso et al., 1989; Tomer et al., 1988). The energy profiles as a function of the side chain torsional angles ψ_1 (C_2-S), ψ_2 (S−CH_2), and ψ_3 (CH_2−CO) displayed minima associated with staggered conformations, with the anti conformers with a slightly lower energy than the gauche conformers and energy barriers ranging from 4 to 20 kcal/mol. As expected, the ψ_4 (CO−Ph) torsional angle showed a preference for symmetrical conformations where the carbonyl is approximately coplanar and eclipsed with the phenyl azide ring. To circumvent the absence of azide parameters, a model for the substituted base lacking the azide was constructed and minimum energy conformations were determined as above. The absence of the azide had little effect on the preferred, calculated structure of the 2-(4-azidophenacyl) analog. Thus, we carried out the furanose conformational studies in the absence of the azide group.

Models for **1** in the C_2'-endo and C_3'-endo conformations were minimized (Kollman All force field), and simulation of the complete pseudorotational cycle of **1** generated an energy profile containing minima at 192 and 345° phase angles (Figure 5); the corresponding furanose ring puckers are C_3'-exo and an unsymmetrical C_2'-exo-C_3'-endo twist, respectively. Conformational analysis of χ as a function of γ defined a clear preference for γ at +sc (60°) and a high anti (−25 to −50°) geometry for χ (Figure 6).

NMR Analysis of Nucleotide Photoprobe Solution Conformation. In the conformational analysis of DNA polymerase photoprobes, the ^3J(H,H) constants for PSEUROT analysis and ROESY experiments were selected. Because a high signal to noise ratio was necessary for accurate ^3J(H,H) determinations, the photoprobe monophosphate was used since (1) sufficient quantities (8−12 mg) could be readily prepared and (2) modeling studies predicted that the α position of the triphosphate had the strongest interaction with the nucleoside. To maintain consistency in the discussion, the monophosphate of **1** is indicated as **1m**.

A global PSEUROT analysis of the ^3J(H,H) couplings of **1m** determined at three temperatures (Table 2) yielded phase

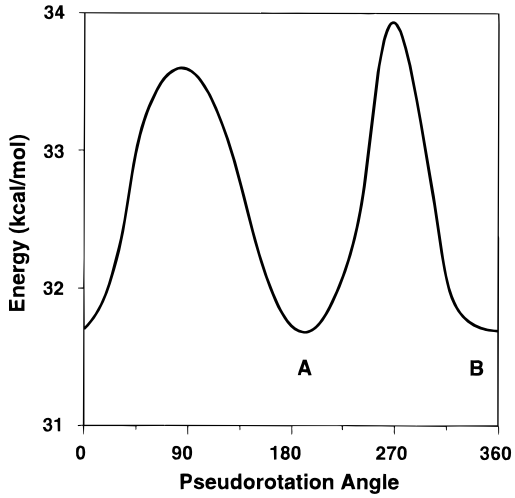

FIGURE 5: Pseudorotational energy profile of **1** as determined from sequential grid searches utilizing the modified Kollman force field minimization procedure in Sybyl.

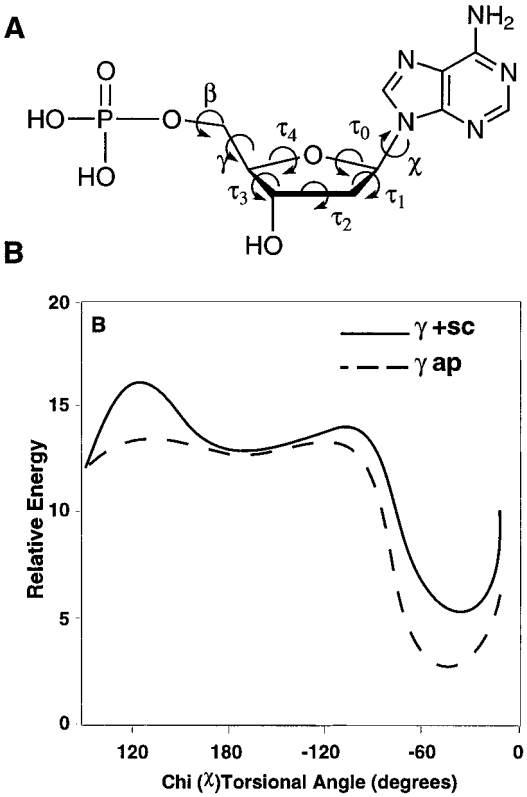

FIGURE 6: (A) Numbering scheme and torsional angle assignment for nucleosides and nucleotides. (B) Energy potential profile of **1** rotated around the torsional angle χ with the γ torsional angle in a +sc (solid line) or ap (dashed line) conformation.

angles of 188.5° (ring pucker of 35.5°, mole fraction of 0.80) and 342.8° (ring pucker of 37.8°, mole fraction of 0.20), corresponding to a C_3'-exo conformation in the major isomer and a C_2'-exo-C_3'-endo twist conformation in the minor isomer; a 0.05 Hz overall rms deviation was observed between the experimental and calculated couplings. The observed sum of the $J_{4'5'}$ and $J_{5'P}$ [i.e., $\sum = (J_{4'5'} + J_{4'5''})$ and $\sum' = (J_{5'P} + J_{5''P})$] values of 6.1 and 9 Hz, respectively, correlates with empirically defined anti-type nucleotides with γ in the +sc form ($\sum = \sim 5-7$ Hz, 60−80% of observed conformations) and β in the ap form ($\sum' = \sim 8-10$ Hz, 70−80% of observed conformations) (Davies, 1978).

Table 2: Coupling Constants for the Furanose Ring Protons of **1m**[a]

	temperature (K)		
couplings	288	298	306
$H_1'-H_2'$	7.40	7.40	7.40
$H_1'-H_2''$	6.10	6.20	6.05
$H_2'-H_3'$	5.80	5.81	5.80
$H_2''-H_3'$	3.00	3.30	3.12
$H_3'-H_4'$	2.20	2.20	2.20

[a] Coupling constants were determined on a Bruker AM 500 instrument in D_2O by sequential decoupling of the furanose protons.

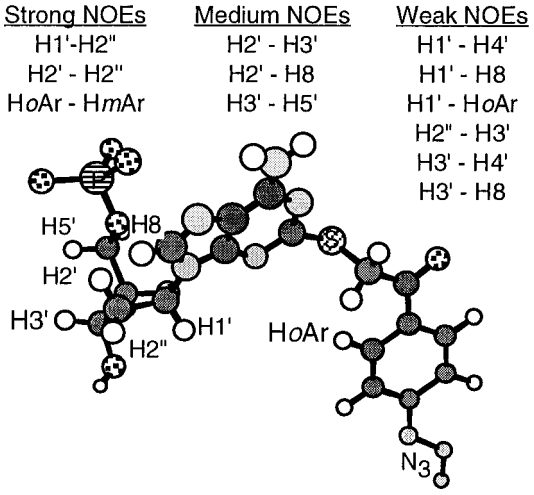

FIGURE 7: (Top) Observed NOE correlations for photoprobe **1**. (Bottom) One calculated energy minimum structure of **1** with a partially extended side chain.

Relative spatial orientations of the protons were examined using ROESY NMR experiments. The experiments were conducted to obtain qualitative distance relationships between protons so NOE enhancements are defined as strong, medium, and weak relative to the intensity of the $C_2'H-C_2''H$ and ArH−ArH′ enhancements, and proton enhancements observed in **1m** (Figure 7) were correlated with the proton distances calculated for the global minima determined in molecular mechanics studies and calculated from PSEUROT analysis of the ^3J(H,H) coupling constants. Using the mean proton distances in each conformer measured with χ at −45°, the medium NOEs occur from 2.5 to 3.5 Å. The very weak cross-peak between H_3' and H_8 probably reflects the major population residing in the C_3'-exo where the calculated distance is 5.1 Å. A weak relaxation enhancement between H_1' and H_{oAr} is evidence that the aromatic ring is not fully extended from the sugar ring, but the absence of NOEs between the ortho and meta protons on the phenyl ring with other sugar protons suggests that the phenyl ring does not reside under the sugar, so the side chain is on average at least partially extended. Although geminal spin relaxation might reduce the intensity, the absence of $H_5'-H_8$ and $H_5''-H_8$ enhancements suggests a +sc conformation since in the ap, C_3'-exo conformation a distance of 4.7 Å should result in a weak but positive enhancement. A medium NOE between H_2' and H_8 and weak NOEs between H_1' and H_8 and H_3' and H_8 are consistent with a χ torsional angle of −45°. In this geometry, the H_8' distance remains relatively constant during C_3'-exo and C_2'-exo-C_3'-endo interconversion relative to H_1' and H_3'.

Molecular Modeling of Photoprobe−Klenow Fragment Interactions. The recently released refined crystal structure

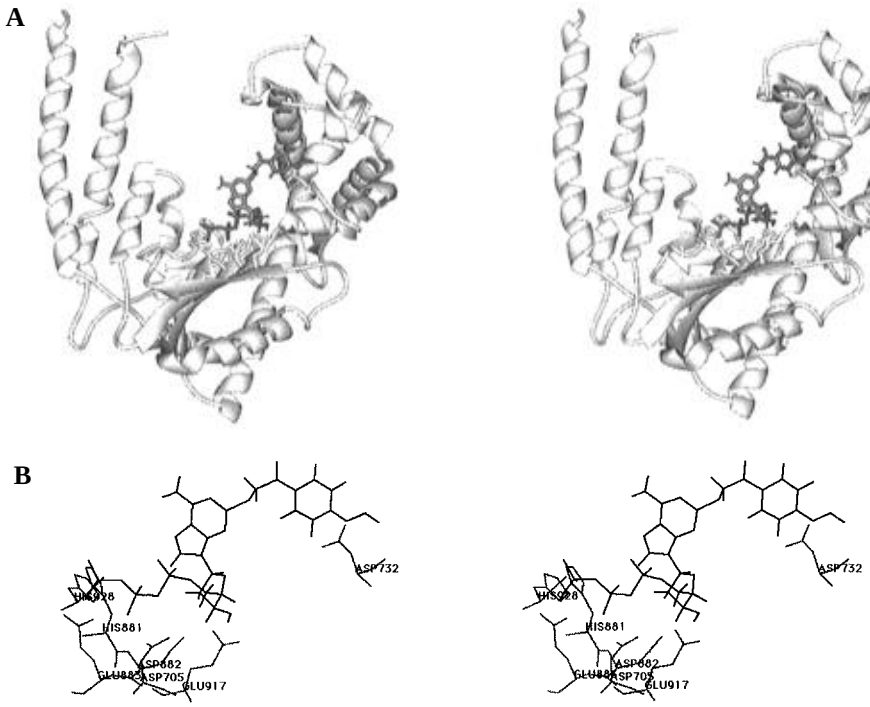

FIGURE 8: Stereopresentation of a model obtained from docking experiments between photoprobe **1** and the Klenow fragment. For clarity, the Klenow fragment is oriented from the side opposite the exonuclease, with the palm region at the bottom, the finger region to the right, and the thumb region to the left: (A) global view generated in MidasPlus and (B) view in the region of major contacts generated in Sybyl.

of the Klenow fragment (Beese et al., 1993a,b) was used in the docking studies. From the photoaffinity labeling experiments, it was known that **1** covalently modifies Asp^{732} on helix N of the Klenow fragment. Utilizing the Asp^{732} carboxylate as an anchor point for the attachment of the α-nitrogen of the aryl azide, energy minima structures of **1** were covalently bound to the enzyme structure. Each complex was rotated about the Asp^{732} Cα−Cβ, Cβ−Cγ, Cγ−O, and O−Nα_{azide} torsional angles in order to move the photoprobe into the enzyme cleft. One such structure prepared from the minimum structure in Figure 7 is presented in Figure 8.

DISCUSSION

In the preceding paper, we outlined our approach to the design of DNA polymerase photoprobes based on the thermodynamic model of DNA polymerase I−substrate interactions (Moore et al., 1996). We proposed to use the triphosphate binding site to anchor a dNTP photoprobe in a catalytic position by tethering an aryl azide into the complementary template binding site. We observed that a three-atom tether is best as compared to a two- or one-atom tether for connecting the aryl azide to a minor groove position of the adenine nucleus. Photoprobe **1** emerged as the best candidate for a photolabel of the Klenow fragment since it photoinactivated the Klenow fragment with saturation and an IC_{50} of about 2 μM. In the present study, we demonstrated that [^{3}H]-**1** photoincorporates into the Klenow fragment, reaching an approximate 1:1 covalent complex at 5.6 μM with an EC_{50} of about 0.75 μM. These results on the photoincorporation of [^{3}H]-**1** into the Klenow fragment correlate with the photoinactivation and kinetic inhibition data published previously (Moore et al., 1996). The approximate free energy of binding calculated from the experimentally determined $K_{D,app}$ is −8.2 kcal/mol, which represents a 1.9−2.3 kcal/mol greater binding energy than that of natural 2′-deoxynucleoside 5′-triphosphates (Englund et al., 1969). Thus, according to our design, the aryl azide of **1** not only is an efficient photolabel but also apparently makes a significant energy contribution to the binding of the photoprobe to the Klenow fragment.

Three lines of evidence suggest that, as designed, photoprobe **1** binds to the triphosphate binding site of the Klenow fragment and that a portion extends into the corresponding template binding site. First, the photoincorporation of [^{3}H]-**1** into the Klenow fragment absolutely requires magnesium, as do substrates that bind to the dNTP binding site (Bryant et al., 1983). Second, the photoincorporation of [^{3}H]-**1** into the Klenow fragment is protected by TTP, a protection that is reversed by high photoprobe concentrations, an observation that suggests a competitive relationship between TTP and the photoprobe. In fact, at a concentration approximately equal to its K_d for the free enzyme form of the Klenow fragment (Englund et al., 1969), TTP shifts the dose−response curve for [^{3}H]-**1** photoincorporation into the Klenow fragment by a factor of approximately 2, and by definition, only a competitive antagonist shifts a dose−response curve by a factor of 2 at its K_d (i.e., $pA_2 = -K_d$) (Schild, 1947). Thus, TTP shows characteristics of a competitive inhibitor of [^{3}H]-**1** photoincorporation, results consistent with our design that photoprobe **1** would anchor to the triphosphate binding site. Third, photoincorporation of [^{3}H]-**1** is inhibited strongly by saturating concentrations of poly(dA)·$(T)_{10}$ (and since the assay for photoincorporation is a DEAE absorption method, the photolabel also does not incorporate into template-primer), evidence that the photolabel binding site also includes the template-primer binding site. Thus, the photoincorporation of [^{3}H]-**1** into the Klenow fragment is clearly efficient, specific, and active site-directed, with binding components in both the template-primer and dNTP binding sites.

Preparative photoaffinity labeling of the Klenow fragment by photoprobe **1** results in a single tryptic fragment containing radioactivity, and we identified Asp^{732} as the site of labeling in helix N of the Klenow fragment. The covalent modification of the Klenow fragment was independently verified by denaturing gel electrophoresis. However, at the first and second HPLC purifications, we recovered only 40 and 35%, respectively, of the incorporated radiolabel. However, this low recovery is not unexpected since it is known that the yield of nucleotide and nucleic acid recovery from reverse phase HPLC can be very low in the absence of ion-pairing solutes (Moore et al., 1996; Williams & Konigsberg, 1991). Additionally, identification of Asp^{732} as the site of covalent modification provides a reasonable explanation for the overall poor recovery of the tryptic fragment. HPLC purification of the peak recovered from the first HPLC purification yielded radioactivity in the void volume as well as the radiolabeled peptide, a result that suggests that the linkage between the peptide and nucleotide was cleaved. Of course, a likely modification of Asp^{732} would be at the carboxylate, through either direct nitrene insertion or nucleophilic attack on a nitrene-derived dehydroazepine (Schuster, 1989), and either of these modifications would yield an ester linkage sensitive to acid hydrolysis.

Recent progress in the modeling of nucleosides and nucleotides provides a powerful tool for predicting the conformational preferences of nucleotide photoprobe **1** for initial enzyme docking studies. Jalluri et al. (1993) added ab initio-determined $C_4'-O_4-C_1'-N_9$ (for purines) torsional parameters to the Kollman force field (which had failed to predict barriers to sugar pseudorotation in grid search techniques) to generate correct barrier heights to nucleoside and nucleotide pseudorotations. This method generated energy profiles for **1** containing minima at 192 and 345° corresponding to C_3'-exo and C_2'-exo-C_3'-endo symmetrical twist conformations, respectively. These low-energy geometries in the pseudorotational cycle have been observed in a number of deoxynucleoside and nucleotide X-ray structures (Saenger, 1973). Additionally, the C_3'-exo sugar pucker is a conformation observed in B-DNA (Arnott & Hukins, 1973). Free pseudorotation of the furanose ring is impeded by 2.4 kcal/mol energy barriers at 90° (eastern barrier) and 270° (western barrier), results consistent with the reported range of 1.6−6 kcal/mol barriers (Govil & Saran, 1971; Jalluri et al., 1993; Jardetzky, 1960; Olson, 1982; Olson & Sussman, 1982). Lowering of the western barrier correlated with favorable van der Waals interactions between the base and phosphate. Additionally, grid searches about χ as a function of γ (+sc or ap) gave minima at −45° and +sc, respectively. These calculated values for C_2'-exo-C_3'-endo (highly restricted) and C_3'-exo furanose conformers were within the defined limits compared to theoretically allowed χ ranges as a function of phase angle (Saran et al., 1973). In combination, the predicted torsional set (i.e., P, χ, and γ) is similar to other nucleotides with furanose puckers of C_3'-exo and C_2'-exo-C_3'-endo.

Modeling studies, although predictive, were not sufficient to establish the solution conformations of the DNA polymerase photoprobe. The use of NMR spectroscopy for determining nucleoside and nucleotide structure has been extensively reviewed (Davies & Danyluk, 1974). Significant information about ring conformation, exocyclic torsional angles, and spatial orientation can be obtained from ^3J(H,H) couplings and NOE effects. Results from such studies reflect equilibrium populations between favorable conformations and therefore can be used as a test of the molecular mechanics results. PSEUROT analysis of the proton coupling constants for **1m** gave a major and minor conformer which confirmed the molecular mechanics studies of a global minimum at 192° with a local minima at 345°, respectively, and the sums of $J_{4'5'} + J_{4'5''}$ and $J_{5'P} + J_{5''P}$ correlate with empirically defined anti-type nucleotides with γ in the +sc form and β in the ap form (Davies, 1978). Additionally, the NOEs observed in the ROESY spectra were consistent with the χ angle in the high anti conformation with a +sc conformation in γ. Thus, the molecular mechanics and NMR conformational analysis of photoprobe **1** predicted similar average solution conformations.

Grid searches about the C_2 side chain torsional angles ψ_1 (C_2-S), ψ_2 ($S-CH_2$), and ψ_3 (CH_2-CO) gave two, three, and three energy minima, respectively, in gauche- or anti-type staggered conformations, providing a combination of 16 preferred low-energy structures. Although there were no side chain proton−proton couplings with which to calculate preferred side chain solution conformations, we used the weak NOE observed between the ortho aromatic proton and the anomeric proton to limit the side chain to eight partially extended low-energy conformers (one of which is illustrated in Figure 7).

These eight low-energy structures of **1** were docked into the active site of the Klenow fragment crystal structure by first connecting the aryl azides' α-nitrogen to the Asp^{732} carboxylate. Since Asp^{732} is some 15−19 Å from the carboxylate triad of Asp^{705}, Asp^{882}, and Glu^{883}, we concluded that the aryl azide of **1** is localized in the template binding region, and thus, we subsequently rotated the photolabel structures toward the carboxylate triad.

The final orientation of **1**, an example of which is given in Figure 8, has several important features which distinguishes it from current models of dNTP binding. First, the base is positioned in the center of the cleft with its minor groove edge across from the N-terminal end of helix O in the finger domain. Second, the 3′-hydroxyl points toward the back of the cleft (away from the exonuclease active site), and the carboxylate of Glu^{917} on β-strand 14 in the back of the palm is within hydrogen-bonding distance of the C_3'-hydroxyl of **1** and occupies a position adjacent to the C_2'H. Third, the triphosphate of **1** readily aligns with Asp^{705}, Asp^{882}, and Glu^{883} in the palm of the Klenow fragment. In one model, a Mg^{2+} ion coordinated to Asp^{705} or Asp^{882} or both would be in position to accept electron density from the α-phosphate or the oxygen bridging the α and β phosphorus atoms (i.e., the atom that accepts electrons during polymerase catalysis). The γ-phosphate group is positioned to interact ionically with His^{881} and His^{928}, and Glu^{883} is positioned to coordinate the Mg^{2+} ion bridging the β- and γ-phosphate anions. Of course, the involvement of Mg^{2+} ions in this model is entirely consistent with the result that magnesium is absolutely required for photoincorporation of [^{3}H]-**1** into the Klenow fragment. Additionally, these potential functions for residues of the carboxylate triad have been proposed in several models of DNA polymerase catalysis (Joyce & Steitz, 1994; Pelletier et al., 1994). In addition to the above interactions of the nucleotide base, sugar, and phosphate, the site of photoaffinity labeling on helix N resides near a hydrophobic pocket formed by the M, N, and O helical

bundle, and this pocket may be a site of interaction by the photolabel side chain.

The proposed orientation of **1** in the Klenow fragment is distinctly different from models of nucleoside triphosphate binding proposed on the basis of earlier results. Thus, two studies suggest that Tyr^{766} is an important residue for dNTP binding; 8-azido-dATP covalently modifies Tyr^{766} (Rush & Konigsberg, 1990), and NOEs have been observed between aromatic residues in the Klenow fragment (presumably at Tyr^{766}) and bound dNTPs (Mullen et al., 1990). Additionally, dNTP substrates occupy positions in the DNA binding cleft in a cocrystal structure such that the triphosphate and base are positioned to interact with charged residues and Tyr^{766}, respectively, on helix O (Beese et al., 1993b). However, in part because the α-phosphate is >6 Å from the carboxylate triad, these authors questioned the significance of this structure to the catalytically competent ternary complex. Recent site-directed mutagenesis studies from separate laboratories suggest instead that Tyr^{766} has a small, indirect effect on dNTP binding in the ternary complex since mutation of this residue decreases the K_m for dNTP by only 2−3-fold (Astatke et al., 1995; Desai et al., 1994; Polesky et al., 1992). Our model also does not accommodate an arrangement of the nucleoside triphosphate along helix O.

Our model of the dNTP binding site in the Klenow fragment is consistent with the thermodynamic model of substrate binding to the Klenow fragment, where the major interaction of the Klenow fragment with dNTP is with the triphosphate (Yadav et al., 1992b), permitting the base to freely interact with the template based on Watson−Crick base pairing. Our labeling studies also support mutagenesis (Astatke et al., 1995; Pandey et al., 1994b) and DNA photolabeling (Pandey et al., 1994a) studies which conclude that residues on helices N and O form contacts with the template strand. Identification of helix N as a site of labeling by **1** places Lys^{758}, Arg^{754}, and Arg^{755} in helix O (which are just above helix N) and His^{734} on helix N adjacent to the phosphodiester bridges of the template 3′ and 5′ to the base complementary to the incoming dNTP. Thus, the geometry of these basic residues is consistent with a role in restraining the orientation of the template at the site of dNTP binding. Additionally, our studies support the proposed roles of Asp^{705}, Asp^{882}, Glu^{883}, and at least two Mg^{2+} ions in Klenow polymerase catalysis (Beese et al., 1993a; Joyce & Steitz, 1994; Polesky et al., 1992; Sawaya et al., 1994) and the orientation of the incoming template-primer proposed by Steitz and colleagues (Beese et al., 1993a; Steitz et al., 1994), i.e., template-primer enters the polymerase active site from the 3′−5′ exonuclease side of the cleft. Our model suggests that dNTPs enter the active site from the opposite end of the cleft, i.e., the side opposite the exonuclease site, and that Glu^{917} on β-strand 14 is part of the dNTP C_3'-hydroxyl binding site.

In conclusion, photoprobe **1** was designed on the basis of the hypothesis that an aryl azide tethered to the minor groove side of a dNTP could make specific contact with the template binding region of the Klenow fragment, thus anchoring the photoprobe into the dNTP binding cleft. The Klenow fragment inhibitory activity of these photoprobes depends on the tether length, with photoprobe **1** showing the highest affinity (Moore et al., 1996). The evidence clearly shows that the enzyme forms a binary complex with photoprobe **1** with an affinity seen with dNTP substrates only in the ternary complex. Additionally, since the covalent photoincorporation of **1** into the Klenow fragment is protected competitively by dNTP and by template-primer substrates, the photoprobe has the properties expected of a bisubstrate inhibitor. Thus, we conclude that the photoinactivation (Moore et al., 1996), photoincorporation, substrate protection, and ion depletion studies provide strong evidence that this proposed binding site for **1** is a good model of the dNTP binding site.

REFERENCES

Altona, C., & Sundaralingam, M. (1972) *J. Am. Chem. Soc. 94*, 8205−8212.

Arnott, S., & Hukins, D. W. L. (1973) *J. Mol. Biol. 81*, 93−105.

Astatke, M., Grindley, N. D. F., & Joyce, C. M. (1995) *J. Biol. Chem. 270*, 1945−1954.

Bambara, R. A., Uyemura, D., & Lehman, I. R. (1976) *J. Biol. Chem. 251*, 4090−4094.

Bambara, R. A., Uyemura, D., & Choi, T. (1978) *J. Biol. Chem. 253*, 413−423.

Beese, L. S., Derbyshire, V., & Steitz, T. A. (1993a) *Science 260*, 352−355.

Beese, L. S., Friedman, J. M., & Steitz, T. A. (1993b) *Biochemistry 32*, 14095−14101.

Brown, W. E., Stump, K. H., & Kelley, W. S. (1982) *J. Biol. Chem. 257*, 1965−1972.

Bryant, F. R., Johnson, K. A., & Benkovic, S. J. (1983) *Biochemistry 22*, 3537−3546.

Carroll, S. S., & Benkovic, S. J. (1990) *Chem. Rev. 90*, 1291−1307.

Davies, D. B. (1978) *Prog. Nucl. Magn. Reson. Spectrosc. 12*, 135−225.

Davies, D. B., & Danyluk, S. S. (1974) *Biochemistry 13*, 4417−4434.

Davies, D. R., & Corbridge, D. E. G. (1958) *Acta Crystallogr. 11*, 315−319.

Delarue, M., Poch, O., Tordo, N., Moras, D., & Argos, P. (1990) *Protein Eng. 3*, 461−467.

Desai, S. D., Pandey, V. N., & Modak, M. J. (1994) *Biochemistry 33*, 11868−11874.

Englund, P. T., Huberman, J. A., Jovin, T. M., & Kornberg, A. (1969) *J. Biol. Chem. 244*, 3038−3044.

Ferrin, T. E., Huang, C. C., Jarvis, L. E., & Langridge, R. (1988) *J. Mol. Graphics 6*, 13−27.

Govil, G., & Saran, A. (1971) *J. Theor. Biol. 33*, 399−406.

Jalluri, R. K., Yuh, Y. H., & Taylor, E. W. (1993) in *The anomeric effect and associated stereoelectronic effects* (Thatcher, G. R. J., Ed.) 277−293, American Chemical Society, Washington, DC.

Jardetzky, C. D. (1960) *J. Am. Chem. Soc. 82*, 229−233.

Joyce, C. M., & Steitz, T. A. (1994) *Annu. Rev. Biochem. 63*, 777−822.

Joyce, C. M., Kelly, W. S., & Grindley, N. D. (1982) *J. Biol. Chem. 257*, 1958−1964.

Klenow, H., Overgaard-Hansen, K., & Patkar, S. A. (1971) *Eur. J. Biochem. 22*, 371−381.

Kornberg, A., Lehman, I. R., Bessman, M. J., & Simms, E. S. (1956) *Biochim. Biophys. Acta 21*, 197−198.

Laemmli, U. K. (1958) *Biochem. J. 68*, 244−251.

Levitt, M., & Warshel, A. (1978) *J. Am. Chem. Soc. 100*, 2607−2613.

Lumbroso, H., Bertin, D. M., Olivato, P. R., Bonfada, E., Mondine, M. G., & Hase, Y. (1989) *J. Mol. Struct. 212*, 113−122.

Mizrahi, V., Henrie, R. N., Marlier, J. F., Johnson, K. A., & Benkovic, S. J. (1985) *Biochemistry 24*, 4010−4018.

Montaudo, G., Finocchiaro, P., Trivellone, E., Bottino, F., & Maravigna, P. (1971) *Tetrahedron 27*, 2125−2131.

Moore, B. M., Li, K., & Doughty, M. B. (1996) *Biochemistry 35*, 11634−11641.

Mullen, G. P., Vaughn, J. B., Shenbagamurthi, P., & Mildvan, A. S. (1990) *Biochem. Pharmacol. 40*, 69−81.

Ollis, D. L., Brick, P., Hamlin, R., Xuong, N. G., & Steitz, T. A. (1985) *Nature 313*, 762−766.

Olson, W. (1982) *J. Am. Chem. Soc. 104*, 278−286.

Olson, W., & Sussman, J. L. (1982) *J. Am. Chem. Soc. 104*, 270−278.
Pandey, V. N., & Modak, M. J. (1988) *J. Biol. Chem. 263*, 6068−6073.
Pandey, V. N., Williams, K. R., Stone, K. L., & Modak, M. J. (1987) *Biochemistry 26*, 7744−7748.
Pandey, V. N., Kaushik, N., & Modak, M. J. (1994a) *J. Biol. Chem. 269*, 21828−21834.
Pandey, V. N., Kaushik, N., & Modak, M. J. (1994b) *J. Biol. Chem. 269*, 13259−13265.
Pelletier, H. (1994) *Science 266*, 2025−2026.
Pelletier, H., Sawaya, A., Kumar, S. H., & Kraut, W. J. (1994) *Science 264*, 1891−1903.
Polesky, A. H., Steitz, T. A., Grindley, N. D. F., & Joyce, C. M. (1990) *J. Biol. Chem. 265*, 14579−14591.
Polesky, A. H., Dahlberg, M. E., Benkovic, S. J., Grindley, N. D. F., & Joyce, C. M. (1992) *J. Biol. Chem. 267*, 8417−8428.
Rush, J., & Konigsberg, W. H. (1990) *J. Biol. Chem. 265*, 4821−4827.
Saenger, W. (1973) *Angew. Chem., Int. Ed. Engl. 12*, 591−601.
Saran, A., Perahia, D., & Pullman, B. (1973) *Theor. Chim. Acta 30*, 31−44.
Sawaya, M. R., Pelletier, H., Kumar, A., Wilson, S. H., & Kraut, J. (1994) *Science 264*, 1930−1935.
Schild, H. O. (1947) *Br. J. Pharmacol. 2*, 189−196.
Schuster, G. B. (1989) in *Photochemical Probes in Biochemistry* (Nielson, P. E., Ed.) pp 31−41, Kluwer Academic, Copenhagen.
Shelton, K. R., & Clark, J. M. (1967) *Biochemistry 6*, 2735−2739.
Sorriso, S., Reichenbach, G., Santini, S., & Ceccon, A. (1974) *J. Chem. Soc., Perkin Trans. 2*, 1588−1590.
Steitz, T. A., Smerdon, S. J., Jager, J., & Joyce, C. M. (1994) *Science 266*, 2022−2025.
Tomer, J. L., Spangler, L. H., & Pratt, D. W. (1988) *J. Am. Chem. Soc. 110*, 1615−1617.
Westhof, E., & Sundaralingam, M. (1980) *J. Am. Chem. Soc. 102*, 1493−1500.
Williams, K. R., & Konigsberg, W. H. (1991) *Methods Enzymol. 208*, 516−539.
Yadav, P. N., Yadav, J. S., & Modak, M. J. (1992a) *Biochemistry 31*, 2879−2886.
Yadav, P. N. S., Yadav, J. S., & Modak, M. J. (1992b) *J. Biomol. Struct. Dyn. 10*, 331−316.

BI952515M